BJU Int 2021; **128:** 178–186 doi:10.1111/bju.15355

Original Article

BJUI
BJU International

Defining prostate cancer size and treatment margin for focal therapy: does intralesional heterogeneity impact the performance of multiparametric MRI?

Edwin Jonathan Aslim[1], Yu Xi Terence Law[2], Stephanie Man Chung Fook-Chong[3], Henry Sun Sien Ho[1], John Shyi Peng Yuen[1], Weber Kam On Lau[1], Lui Shiong Lee[4], Christopher Wai Sam Cheng[4], Nye Thane Ngo[5], Yan Mee Law[6] and Kae Jack Tay[1]

[1]*Department of Urology, Singapore General Hospital,* [2]*Department of Urology, National University Hospital,* [3]*Health Services Research Unit, Singapore General Hospital,* [4]*Department of Urology, Sengkang General Hospital,* [5]*Department of Anatomical Pathology, Singapore General Hospital, and* [6]*Department of Diagnostic Radiology, Singapore General Hospital, Singapore City, Singapore*

N.T.N, Y.M.L, and K.J.T. contributed equally to this work.

Objectives

To evaluate the impact of intralesional heterogeneity on the performance of multiparametric magnetic resonance imaging (mpMRI) in determining cancer extent and treatment margins for focal therapy (FT) of prostate cancer.

Patients and Methods

We identified men who underwent primary radical prostatectomy for organ- confined prostate cancer over a 3-year period. Cancer foci on whole-mount histology were marked out, coding low-grade (LG; Gleason 3) and high-grade (HG; Gleason 4–5) components separately. Measurements of entire tumours were grouped according to intralesional proportion of HG cancer: 0%, <50% and ≥50%; the readings were corrected for specimen shrinkage and correlated with matching lesions on mpMRI. Separate measurements were also taken of HG cancer components only, and correlated against entire lesions on mpMRI. Size discrepancies were used to derive the optimal tumour size and treatment margins for FT.

Results

There were 122 MRI-detected cancer lesions in 70 men. The mean linear specimen shrinkage was 8.4%. The overall correlation between histology and MRI dimensions was $r = 0.79$ ($P < 0.001$). Size correlation was superior for tumours with high burden (≥50%) compared to low burden (<50%) of HG cancer ($r = 0.84$ vs $r = 0.63$; $P = 0.007$). Size underestimation by mpMRI was more likely for larger tumours (51% for >12 mm vs 26% for ≤12 mm) and those containing HG cancer (44%, vs 20% for LG only). Size discrepancy analysis suggests an optimal tumour size of ≤12 mm and treatment margins of 5–6 mm for FT. For tumours ≤12 mm in diameter, applying 5- and 6-mm treatment margins would achieve 98.6% and 100% complete tumour ablation, respectively. For tumours of all sizes, using the same margins would ablate >95% of the HG cancer components.

Conclusions

Multiparametric MRI performance in estimating prostate cancer size, and consequently the treatment margin for FT, is impacted by tumour size and the intralesional heterogeneity of cancer grades.

Keywords

focal therapy, cancer size, treatment margin, high grade, multiparametric MRI, prostate cancer, #ProstateCancer, #PCSM, #uroonc

Introduction

The advent of multiparametric MRI (mpMRI) and MRI–ultrasonography fusion targeted biopsy have enabled urologists to accurately map the location of clinically significant cancer within the prostate [1]. Although some cancer lesions may be missed on mpMRI, the rate of underdetection is low [2]. This has led to increased interest in

focal therapy (FT) of the malignant focus, sparing benign adjacent tissue to minimize collateral damage to important functional structures [3]. While mpMRI has good performance in cancer detection, it is lacking in determining cancer *extent* in localized disease; some authors have reported discrepancies between the tumour dimensions on MRI and histology [4,5].

Concerns with cancer persistence have resulted in recommendations for a large treatment margin to completely ablate the malignant focus. Prostate cancer is often heterogenous, and different theories on cancer progression have been put forward to explain this; the clonal model proposes that the cancer components of different grades exist and grow separately, while the transitional model describes the same population of cancer cells progressing from low grade (LG) to high grade (HG) [6,7]. The impact of intralesional heterogeneity on mpMRI performance in determining the extent and margin for cancer ablation has not been studied. Low-risk prostate cancer (PSA < 10 ng/mL, Gleason score 6, cT2a) is highly amenable to expectant management, with very low metastatic and mortality rates at 10–15 years [8,9]. In a recent expert consensus, the stated goal of FT is to eradicate clinically significant cancer, through treatment and repeated treatments, to potentially defer radical therapy indefinitely [10]. In this paradigm, patients with small, ablatable volumes of Gleason score (GS) >6 cancer might be treated with FT, even with small amounts of viable GS 6 cancer at the treatment margin, as their disease is 'downgraded' to a low-risk status. Currently, there exists no evidence-based standard of care on how wide these treatment fields ought to be. Data from some studies have suggested that the margins could be approximately 9–10 mm, but these studies compared tumour sizes as a whole without differentiating between the LG and clinically important HG components [4,11].

We postulate that mpMRI is excellent in detecting HG cancer (Gleason grade 4 and 5), but lacking in the detection of LG cancer (Gleason grade 3). We aim to determine and compare the performance of mpMRI in defining the size of the entire cancerous lesion or the HG components only, to determine the ideal tumour size and treatment margin for FT.

Patients and Methods

Patient Cohort

An institutional review board approval (CIRB: 2017/2651) and waiver of informed consent were obtained for this study. All men who underwent radical prostatectomy as primary treatment for organ-confined adenocarcinoma of the prostate between 1 January 2015 and 31 December 2017 were identified from our prospectively maintained Urology Cancer Registry (UroCaRe) database. Only those with available whole-mount histology and mpMRI performed within our institution, either pre-biopsy or at least 1 year from a previous prostate biopsy, were included. This was to remove the effects of post-biopsy haemorrhage on MRI performance. Patients who had previous surgery to the prostate, androgen deprivation therapy, pelvic irradiation and pelvic metalwork were excluded from analysis.

Multiparametric MRI Data Acquisition

All patients underwent a high-field mpMRI examination without an endorectal coil, using a 3-Tesla MRI imaging system (Magnetom Skyra; Siemens, Erlangen, Germany) with a multichannel pelvic phased-array coil. The image acquisition protocols are shown in Table S1. The intravenous contrast agent was gadoterate meglumine (DOTAREM®; Guerbet LLC, Bloomington, IN, USA), injected at a dose of 0.1 mmol/kg body weight and a rate of 2–3 mL/s, followed by a 20-mL saline flush. Images were retrospectively reviewed on a commercial PACS workstation (Carestream, Rochester, NY, USA), and assessed by a senior genitourinary radiologist (L.Y.M.) with 8 years of experience in reading prostate MRI, who was blinded to the histology findings. Each lesion was scored according to the Prostate Imaging-Reporting and Data System (PI-RADS) version 2 criteria [12], and the measurements were taken primarily on the T2-weighted imaging sequences in the axial plane.

Histopathological Preparation

Each radical prostatectomy specimen was fixed in formalin according to a standardized regime for a total of 48 h before processing. Upon receipt, the specimen was fixed in formalin for 24 h, then subjected to routine macroscopic examination and orientation. The vas and seminal vesicles were amputated close to the prostate base and entirely embedded. Sections from the apex and base were taken perpendicular to the urethra. These sections were then sliced sagittally. The rest of the prostate was sliced into 3.5-mm whole-mount sections (with the help of a guide), perpendicular to the urethra and embedded sequentially. The entire prostatectomy specimen was embedded and placed in cassettes, which were fixed in formalin for an additional 24 h, before loading into the processing machines. Each cancer focus was dotted out with indelible ink (Staedtler Lumocolor fine-tip marker 0.6-mm width), coding LG (Gleason grade <4) and HG (Gleason grade 4–5) components in different colours. Malignant foci <1 mm apart in the same plane were considered part of the same lesion. A lesion was categorized as anterior in location if ≥75% of the tumour was anterior to the urethra. All whole-mount histology sections were reviewed by a senior uro-pathologist (N.N.T.) with 9 years of experience in genitourinary pathology.

Correcting for Specimen Shrinkage on Histology

Formalin-related linear specimen shrinkage was determined by making comparisons between the maximal side-to-side prostate diameters on MRI and histology, in the axial planes. All histology measurements were corrected for specimen shrinkage using the mathematical formulas:

$$\text{Shrinkage factor (SF)} = \frac{\text{MRI PD} - \text{histology PD}}{\text{MRI PD}}$$

$$\text{Corrected tumour size} = \frac{\text{measured tumour size}}{1 - \text{SF}},$$

where PD is prostate diameter.

Measuring and Defining Lesion Size

Cancer size was determined by using the lesion diameter. Lesions on MRI and histology were matched, and then measured in the same axial cuts in two sets of orientations (Fig. 1). The 'systematic' dimensions were the averaged vertical and horizontal measurements, while the 'best-fit' dimensions were the averaged measurements of two longest diameters perpendicular to each other. The representative size of a lesion was its composite dimension, which was derived by averaging all measurements (systematic and best fit).

To evaluate whether different measurement techniques pose a significant impact on size estimation, the systematic and best-fit dimensions were compared within each method (i.e. MRI or histology) using the intraclass correlation coefficient (ICC) measure. To evaluate the accuracy of MRI in determining cancer size and treatment margins, the composite dimensions were compared between the methods.

Defining Treatment Margins

The concept of treatment margin is to plan a wider treatment field to treat those tumours that are underestimated in size by MRI (i.e. larger on histology). We derived the treatment margins based on the discrepancies in composite tumour diameters on histology and MRI. To assess if the treatment margins would adequately treat clinically significant cancer, we compared the composite diameters of HG components only on histology against entire lesions on MRI.

Defining Size Underestimation by MRI

We defined MRI size underestimation as all tumours that were measured to be smaller on MRI vs histology where the size discrepancies were ≥0.5 mm. This threshold was used to

Fig. 1 Multiparametric MRI sequences and whole-mount histology sections of the same prostate gland taken in the same axial plane. Arrowheads identified the index (right anterior) and satellite (left lateral) lesions on (**A**) T2-weighted imaging, (**B**) apparent diffusion coefficient map, and (**C**) diffusion-weighted imaging. (**D**) Index lesion measured in 'systematic' (yellow lines) and 'best-fit' (green dashed lines) orientations. (**E, F**) Prostate cancer on whole-mount sections were marked out in different colours to discriminate between low-grade (blue) and high-grade (HG; black) components, and then measured in the same manner for (**E**) whole lesion and (**F**) HG only.

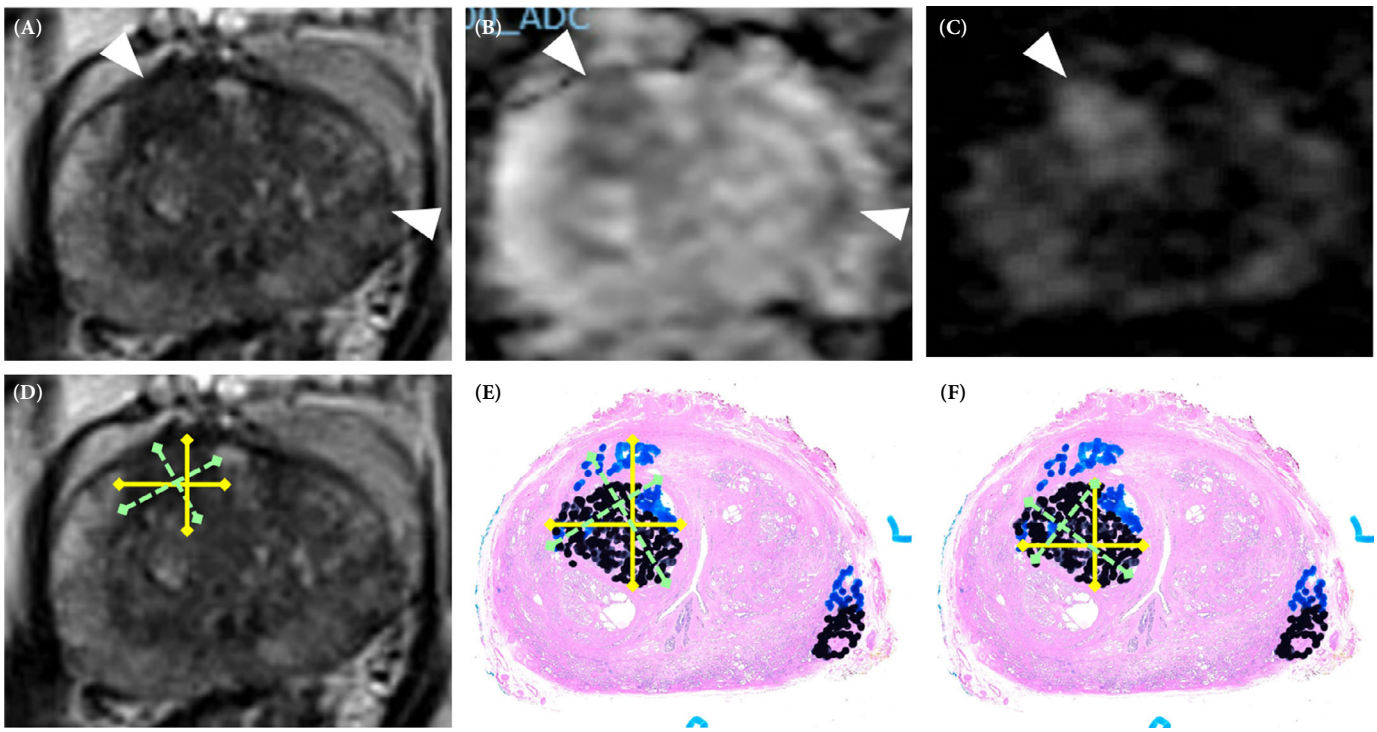

account for potential human errors, as 0.5 mm represents the degree of uncertainty for measurements made with a millimetre ruler.

Intralesional Heterogeneity Evaluation

On the whole-mount slide showing the largest section of a tumour lesion, the proportion of HG cancer for that lesion was calculated, based on size comparisons or, in cases where the HG components were interspersed among LG cancer, visual estimation. The tumour lesions were then grouped according to their HG cancer content: HG0 (no HG cancer present), HG1 (<50% HG cancer present) and HG2 (≥50% HG cancer present). We defined high-burden of HG cancer as ≥50% (HG2) and low-burden as <50% (HG0 and HG1). Histology–MRI size comparisons were assessed for differences between the groups.

Statistical Analysis

The ICC was used to evaluate the agreement between different measurement techniques by one method. Cancer lesions on MRI and histology were matched, and correlated for size using the Pearson correlation. The plots of MRI–histology size differences against tumour size on histology were used to assess size discrepancies and to calculate the optimal tumour size and treatment margins for FT. The impact of intralesional heterogeneity on mpMRI performance was assessed using linear regression of MRI size with pathology size and HG cancer burden, and their interaction as independent predictors. Categorical data were compared between groups using the chi-squared test and continuous data were tested using the two-tailed Student's *t*-test. Statistical significance was defined as $P < 0.05$. The statistical software used was IBM SPSS Statistics for Windows version 25.0 (IBM Corp., Armonk, NY, USA) and MedCalc version 18.2 (MedCalc Software, Ostend, Belgium).

Results

Patient and Prostate Characteristics

We identified 70 suitable patients, with the characteristics as summarized in Table 1. mpMRI was performed pre-biopsy in 60% (42/70) and more than 1 year post biopsy in 40% of patients (28/70). The mean (SD) specimen shrinkage was 8.4 (5.4)%.

Table 1 Patient and prostate characteristics.

Number of patients	70
Median (IQR) age, years	65 (61–69)
Median (IQR) PSA, ng/mL	8.3 (6.3–10.9)
Median (IQR) PSA density, ng/mL^2	0.21 (0.16–0.40)
ISUP grade group, *n* (%)	
1 (GS 6)	7 (10)
2 (GS 3 + 4)	42 (60)
3 (GS 4 + 3)	17 (24)
4 (GS 8)	2 (3)
5 (GS 9–10)	2 (3)
Pre-biopsy MRI, *n* (%)	42 (60)
Post-biopsy >1-year MRI, *n* (%)	28 (40)
Mean (SD) MRI-PV, mL	39.5 (16.8)
Mean (SD) linear shrinkage, %	8.4 (5.4)
MRI suspicious lesions, *n*	169
Cancer foci on histology, *n*	160
MRI true-positive cancer, *n*	122

GS, Gleason score; MRI-PV, MRI-estimated prostate volume; IQR, interquartile range; ISUP, International Society of Urological Pathology (2014).

Evaluation of Multiparametric MRI in Prostate Cancer Detection

There were 160 histology-confirmed cancer foci and 169 mpMRI-detected suspicious lesions. MRI true positives comprise 122 lesions, giving mpMRI a sensitivity of 76% (95% CI 0.69–0.83) and a positive predictive value of 72% (95% CI 0.64–0.78) for cancer detection. The false-positive rate was 28%.

Intralesional Heterogeneity

Out of the 122 MRI true positives, approximately half (52%, $n = 63$) were non-heterogenous, being either entirely LG or HG. The distributions of the tumours were as follows: 34% ($n = 41$) were homogenously LG; 18% ($n = 22$) had <50% HG cancer; 30% ($n = 37$) had ≥50% to <100% HG cancer; and 18% ($n = 22$) were homogenously HG. Out of the 59 heterogenous tumours, 63% had ≥50% HG cancer and 37% had <50% HG cancer components. Tumours with a high burden of HG cancer comprised 48% of all cancer, while HG cancer was present in 66% of all cancer.

Size Correlations Between MRI and Histology

The lesion measurements are summarized in Table 2. Assessing the agreement between systematic and best-fit dimensions, the ICC for MRI was 0.992 (95% CI 0.984–0.996; $P < 0.001$) and for histology it was 0.994 (95% CI 0.992–0.996; $P < 0.001$); the high ICC value implied that measurement methods had no significant impact on the working size of each lesion.

Impact of Intralesional Heterogeneity

The correlation coefficient between the composite dimensions on MRI and histology was $r = 0.79$ (95% CI 0.72–0.85; $P < 0.001$). Tumours with high burden of HG cancer had better size correlation ($r = 0.84$, 95% CI 0.75–0.90; $P < 0.001$) as compared to those with low burden ($r = 0.63$, 95% CI 0.46–0.76; $P < 0.001$ [Fig. 2]), with a P value of 0.007 for significant interaction between HG cancer burden and pathology diameter on linear regression. Larger tumours had

Table 2 Intralesional heterogeneity groups: lesion characteristics.

Intralesional groupings	Mean (SD) lesion size, mm		Size correlation		Distribution by tumour size, % (*n*)			Location, % (*n*)			MRI underestimation by tumour size, % (*n*)			
	MRI	Histology	*r*	*P*	≤12 mm	>12 mm	*P* *	Anterior	Non-anterior	*P*	All size	≤12 mm	>12 mm	*P**
All lesions	11.0 (4.9)	10.6 (6.1)	0.79	<0.001	60 (73)	40 (49)	0.002	64 (77)	37 (45)	<0.001	36 (44/122)	26 (19/73)	51 (25/49)	0.005
HG0	8.2 (2.8)	5.9 (3.6)	0.55	<0.001	90 (37)	10 (4)	<0.001	51 (21)	49 (20)	0.8	20 (8/41)	14 (5/37)	75 (3/4)	0.004
HG1	11.5 (4.1)	12.7 (3.8)	0.48	0.02	41 (9)	59 (13)	0.2	77 (17)	23 (5)	<0.001	50 (11/22)	44 (4/9)	54 (7/13)	0.9
HG2	12.7 (5.5)	13.2 (6.3)	0.84	<0.001	46 (27)	54 (32)	0.4	68 (40)	32 (19)	0.006	42 (25/59)	37 (10/27)	47 (15/32)	0.5
HG0 + HG1	9.4 (3.6)	8.3 (4.9)	0.63	<0.001	73 (46)	27 (17)	<0.001	69 (37)	41 (26)	0.05	30 (19/63)	20 (9/46)	59 (10/17)	0.01
HG1 + HG2	12.3 (5.1)	13.1 (5.7)	0.79	<0.001	44 (36)	56 (45)	0.2	70 (57)	30 (24)	<0.001	44 (36/81)	39 (14/36)	49 (22/45)	0.4

*HG0, all low-grade cancer; HG1, proportion of high-grade cancer <50%; HG2, proportion of high-grade cancer >50%; HG0 + HG1, low burden of high-grade cancer; HG1 + HG2, all tumours containing high-grade cancer; r, correlation between lesion size on pathology and MRI. * P values from chi-squared tests comparing ≤12 mm vs >12 mm tumours.*

higher content of HG cancer, with mean lesion sizes of 5.9 mm for HG0, 12.7 mm for HG1 and 13.2 mm for HG2 groups of tumours.

Impact of Tumour Location

Of the 122 MRI true-positive cancer foci, 77 (63%) were anterior and 45 (37%) were non-anterior in location. Most of the cancers were found in the peripheral zones of the prostate (71% for anterior and 96% for non-anterior tumours), as shown in Table S2. Among the tumours containing HG cancer, a higher proportion were anteriorly based, as compared to non-anterior in locations (70% vs 30%; $P < 0.001$). There were no statistically significant differences in tumour size based on anterior vs non-anterior locations ($P = 0.258$).

Determination of Optimal Tumour Size and Treatment Margin for Focal Therapy

Plots of the size discrepancies between MRI and histology against tumour size on histology are shown in Fig. 3. The measurement errors were more pronounced at the extremes of size; MRI tended to overestimate smaller and underestimate larger lesions. Visual analysis of the plots against histology suggested that MRI was most accurate for lesions between 8 and 10 mm.

Measurement errors between MRI and histology could occur at either end of a measured diameter; therefore, we conservatively derived the treatment margins based on the absolute differences in lesion diameters. Using this method, for tumour size on histology up to 12 mm ($n = 73$), a 5-mm radial margin would achieve 98.6% (72/73) complete tumour ablation, while a 6-mm margin would achieve 100% complete ablation. For larger tumours (>12 mm), using 5- and 6-mm margins would achieve 85.7% (42/49) and 87.8% (43/49) complete ablation, respectively.

A plot of the size differences between the two methods (HG-only components on histology vs entire lesions on MRI) against entire tumour size on histology suggests that our proposed treatment margins would treat most of the HG cancer. For all tumour sizes, applying a 5-mm margin would ablate 96.3% (78/81), while a 6-mm margin would treat 98.8% (80/81) of the clinically significant cancer components.

Size Underestimation by MRI

Overall, 36% of all tumours were underestimated in size by MRI, with a higher tendency in larger tumours (51% for >12 mm vs 26% for ≤12 mm; $P = 0.005$). For tumours >12 mm, the rates of MRI underestimation were 75% for LG lesions and 49% for HG lesions. While the likelihood for size underestimation by MRI was higher with increasing size, the

Fig. 2 Scatterplot showing the correlation between lesion size on MRI and histology. Red dotted line represents the trend line for high high-grade (HG) cancer burden, and blue dotted line represents the trend line for low HG cancer burden. HG0, all low-grade cancer; HG1, proportion of HG cancer < 50%; HG2, proportion of HG cancer >50%; HG0 + HG1, low burden of HG cancer.

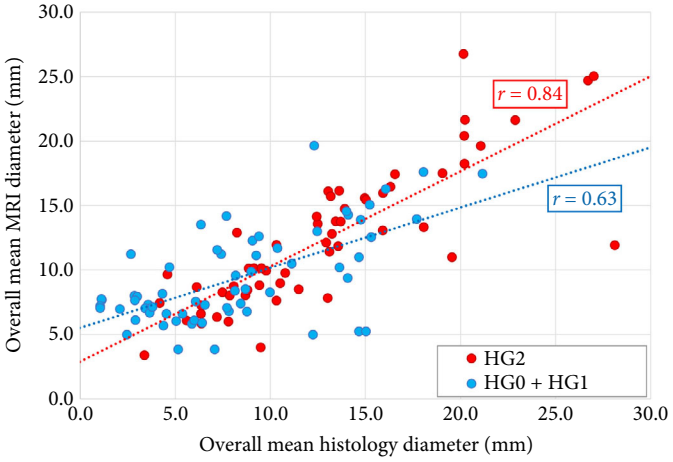

Fig. 3 Plots of size discrepancies (MRI minus histology) against entire tumour size on histology for (**A**) all lesions and (**B**) high-grade (HG) components only. Datapoints above zero on the *y*-axis represent size overestimation by MRI, and vice versa. Blue vertical line represents tumour size at 12 mm. Red lines are theoretical 5 mm (coarse-dotted) and 6 mm (fine-dotted) treatment margins.

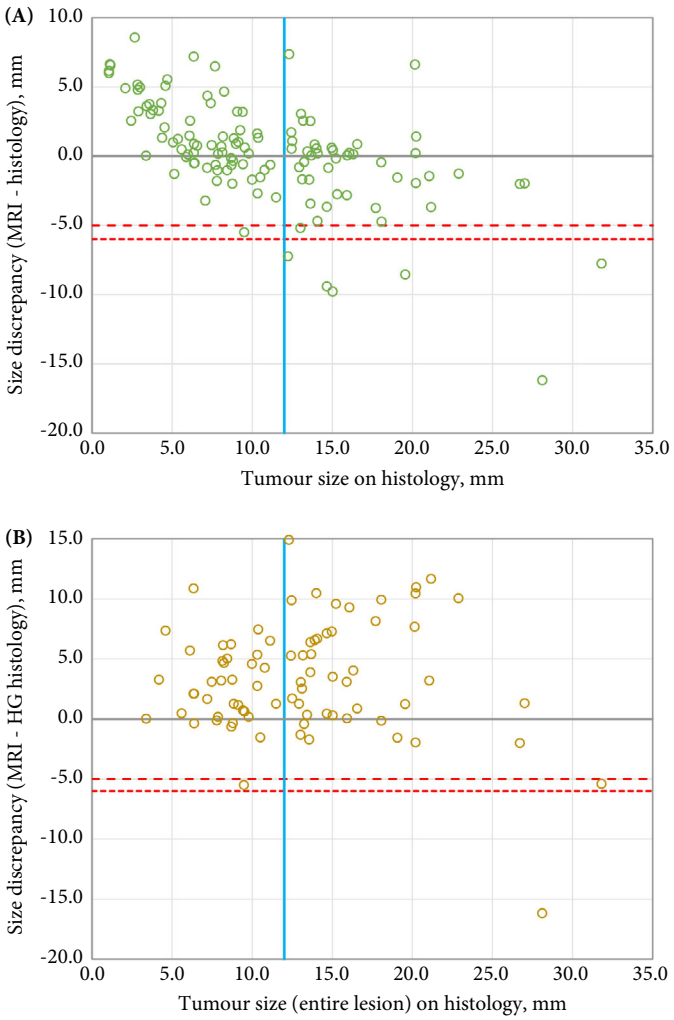

degree of size discrepancies seemed constant when compared against HG-only components on histology (Fig. 3).

The presence of HG cancer was associated with a higher likelihood of underestimation by MRI as compared to LG cancer only (44% for HG1 + HG2 vs 20% for HG0; P = 0.007). Tumours with higher content of HG cancer were more likely to be underestimated than those with lower content (50% for HG1 vs 42% for HG2; P = 0.541), although this was not statistically significant, probably owing to the small sample size.

Characteristics of Cancer Missed on mpMRI

Multiparametric MRI missed 38 cancer lesions, giving a false-negative rate of 24%. The mean (SD) tumour diameter was 4.4 (2.3) mm (95% CI 3.7–5.2,) for MRI-missed lesions vs 10.6 (6.1) mm (95% CI 9.5–11.7) for MRI-detected lesions (P < 0.001). HG cancer was found in 24% (n = 9) of missed lesions. Extrapolating to spherical volumes, the mean tumour volume for MRI-missed lesions was approximately 0.044 mL.

Sub-analysis of Focal Therapy-Suitable Patients

There were 20 patients, comprising 35 tumour foci, who were deemed appropriate candidates for FT, using the selection criteria of up two tumour foci, each measuring up to 1.5 mL (approximately 14.5 mm in diameter) and GS ≤8. Using a 6-mm treatment margin, complete ablation would be achieved in 100% (27/27) of all tumours ≤12 mm and 88% (7/8) of tumours >12 mm size, as shown in Fig. S1.

Discussion

In the present study, we demonstrated good overall concordance between MRI and histology in measuring prostate cancer size. The size underestimation of larger tumours and those containing HG cancer can be problematic, especially when larger tumours were also more likely to harbour a higher burden of HG cancer.

One confounder of the effect of tumour size on MRI underestimation is that MRI occult lesions, which would effectively have been 'underestimated', were by default excluded from analysis. Another explanation could be that the often hazy appearance of cancer margins on mpMRI

might compel the reader to overmeasure the less obvious smaller lesions and underestimate larger ones. The presence of HG cancer might influence the detection of the LG components in heterogenous tumours, such that the measurements were biased for the more obvious HG cancer, ignoring the softer 'halo' of LG cancer. Our data seem to support this by showing that the size discrepancies against HG-only components on histology remained constant, despite the greater magnitude of MRI underestimation with increasing tumour size. In addition, tumours with lower HG cancer content were more likely to be underestimated than those with higher content, in a seemingly contradictory observation to that of the tendency for MRI to underestimate tumours containing HG cancer as compared to entirely LG tumours. Therefore, we postulate that, although mpMRI is better at detecting HG cancer than LG cancer, intralesional heterogeneity has an impact on the performance of mpMRI in determining cancer extent.

In our dataset, we found the optimal tumour size to be less than 12 mm and the optimal treatment margin to be 5–6 mm for FT. These thresholds were interlinked; as MRI measurements became increasingly inaccurate for larger tumours beyond 12 mm, larger treatment margins would be required for tumours beyond this size. Our data suggest that a treatment margin of 5–6 mm would ablate all viable tumours within 12 mm in size, most of the time. For tumours larger than 12 mm, most of the clinically significant cancer would be eradicated, even if the entire tumour was incompletely ablated. In a study using MRI–histology co-registration analysis to determine the three-dimensional (3D) treatment margin, the authors concluded that a 9-mm margin would achieve complete tumour destruction in all cases [11]. The optimal tumour size was not evaluated in that study. This is significant as larger tumours would require wider treatment margins. In a recent expert consensus, tumour size up to 3 mL (approximately 18 mm in diameter) was deemed appropriate for FT [13]. Applying a 9-mm treatment margin would therefore add 18 mm to the treatment diameter, resulting in an extensive ablation field. At the time of writing, there are no studies linking the extent of treatment margin with complication rates; but presumably a wide ablation field would more likely result in injury to the surrounding structures. Such one-size-fits-all strategies seem crude, and refining a more precise treatment algorithm requires improving the imaging accuracy. This may be achieved by incorporating additional clinical variables, such as PSA density, or advances in MRI techniques. In a repeat-biopsy study, PSA density was shown to influence the predictive values of mpMRI in detecting GS $\geq$7 prostate cancer [14]. Good characterization of microstructural tissue compartments in prostate cancer was demonstrated in one MRI whole-mount study using diffusion–relaxation correlation spectrum imaging [15]. In the future, incorporating artificial intelligence into the treatment algorithm could aid prostate cancer diagnosis and treatment planning [16].

Our reported mean linear specimen shrinkage was 8.4%, translating to a volumetric tissue shrinkage of 23.1% and a correction factor of 1.30. This is consistent with other studies, which have published tissue correction factors ranging between 1.14 and 1.50 [17,18]. The sensitivity of mpMRI in the present study for cancer detection was 76%, with a positive predictive value of 72%, which was consistent with other series and our own post-biopsy data [19–21]. MRI-missed cancer lesions were mostly LG and small, measuring under the 0.5-mL size definition for clinically significant cancer proposed by Stamey et al. [22] Offering FT for prostate cancer therefore comes with the caveat that approximately 20% of cancers may be missed by MRI, although these might not be clinically significant.

Various factors can impact FT outcomes, such as MRI reader experience and the extent of ablation, whether targeted or zonal [23]. In an MRI–ultrasonography fusion-guided biopsy study, improved prostate cancer detection over time suggested a learning curve for mpMRI reporting [24]. A review of FT cohort studies found the reported infield, or treated area, cancer persistence rates to be between 10% and 20% at 6–12-month post-treatment biopsy [25]. A highly precise ablation can result in viable cancer at the treatment margins, as demonstrated in one ablate-and-resect study for MRI-guided focal laser ablation [26]. The long-term oncological impact of remnant cancer at the margin after ablation is unknown; nevertheless, remnant HG cancer would be considered treatment failure [27,28]. There is evidence that the index lesion in multifocal tumours represents the truly relevant malignant focus, and satellite tumours are mostly small and LG [29]. Treating only the index lesion can achieve good short-term cancer control, but the long-term outcomes remain uncertain [30]. While the ideal goal would be the complete destruction of all viable cancer, given a robust active surveillance protocol, remnant LG or clinically insignificant cancer may one day be an acceptable option, thus deferring radical therapy and its associated morbidities. Disease recurrence or progression could be treated with repeat ablation or radical treatment.

There are several limitations to this study. First, our proposed margins are applicable for the intra-parenchymal, 'internal' facing aspects of the tumours. The 'external' facing margins towards the edge of the prostate are limited by the natural boundaries of the gland. On the one hand, extending the margins beyond the prostate, especially at the base and apex, could injure critical structures. On the other hand, the presence of extracapsular extension could result in FT failure. Some variables have been established to predict extracapsular extension on prostate MRI [23,31]. With the careful selection of organ-confined disease for FT

cases, cancer beyond the prostate would not be expected. Therefore, ablating the lesions up to the anatomical edge of the prostate could be adequate. Second, our patient cohort was selected for radical prostatectomy, and most cases would not have been eligible for FT outright. We have analysed all tumours on a per-lesion basis to improve the precision of our estimates. Third, using lesion diameter as a surrogate for its size may be overly simplistic. We erred on the conservative side by using the longest lesion diameter, so that the planned ablation field would result in overtreatment rather than undertreatment. Fourth, our calculations for the limits of tumour size and treatment margins were based on histology. In real-life practice, treatment planning is based on preoperative imaging and is subject to the inherent measurement errors of that imaging tool. To avoid compromising the oncological outcomes, we strongly advocate meticulous case selection and appropriate choice of ablation field. Next, the tumour 'depth' measurement was limited by the whole-mount slice thickness; the histology–MRI axial size correlations were assumed extrapolatable to the other planes. The exact matching between MRI and histology cuts were challenging as the slice thickness and segment location could be different, especially when access to good MRI–histology coregistration software was not available. As we did not use a prostate mould, there could be discrepancies in the 'axial' planes between MRI and histology; while the histology slices were typically taken perpendicular to the axis of the prostate gland, the MRI sections were oriented axial to the patient. Also, the calculations of specimen shrinkage could be affected by the tissue thickness, due to errors in the measurements of maximum side-to-side prostate diameters. To minimize this error, we tried keeping the slices between 3 and 5 mm thick; however, there would always be slight variability in tissue thickness despite best efforts, as has been reported by other authors [15]. Our specimen shrinkage calculations did not account for non-uniform distortions of the prostate in 3D. Indeed, such distortions were demonstrated in a study comparing radical prostatectomy specimens with 3D-printed patient-specific prostate moulds modelled using preoperative MRI [4].

In conclusion, our study exposes the influence of intralesional heterogeneity on mpMRI performance in determining prostate cancer extent. HG lesions tend to be larger and have better size correlations with MRI, but at the same time are more likely to be underestimated. Consequently, the treatment margin during FT may vary depending on these factors. While our observations suggest that FT with a treatment margin of 5–6 mm for a tumour up to 12 mm in size would achieve complete ablation of the lesion, further data on long-term oncological outcomes are needed.

Acknowledgements

We would also like to thank the Urology Department at Singapore General Hospital for their support in completing this study. The authors received no financial support for the research, authorship, and publication of this paper.

Conflict of Interest

None declared.

References

1 **Siddiqui MM, Rais-Bahrami S, Turkbey B et al.** Comparison of MR/ultrasound fusion-guided biopsy with ultrasound-guided biopsy for the diagnosis of prostate cancer. *JAMA* 2015; 313: 390–7

2 **Bryant RJ, Hobbs CP, Eyre KS et al.** Comparison of prostate biopsy with or without prebiopsy multiparametric magnetic resonance imaging for prostate cancer detection: an observational cohort study. *J Urol* 2019; 201: 510–9

3 **Ganzer R, Arthanareeswaran VKA, Ahmed HU et al.** Which technology to select for primary focal treatment of prostate cancer?—European Section of Urotechnology (ESUT) position statement. *Prostate Cancer Prost Dis* 2018; 21: 175–86

4 **Priester A, Natarajan S, Khoshnoodi P et al.** Magnetic resonance imaging underestimation of prostate cancer geometry: use of patient specific molds to correlate images with whole mount pathology. *J Urol* 2017; 197: 320–6

5 **Cornud F, Khoury G, Bouazza N et al.** Tumor target volume for focal therapy of prostate cancer-does multiparametric magnetic resonance imaging allow for a reliable estimation? *J Urol* 2014; 191: 1272–9

6 **Esserman L, Shieh Y, Thompson I.** Rethinking screening for breast cancer and prostate cancer. *JAMA* 2009; 21: 1685–92

7 **Lavery HJ, Droller MJ.** Do Gleason patterns 3 and 4 prostate cancer represent separate disease states? *J Urol* 2012; 188: 1667–75

8 **Klotz L, Vesprini D, Sethukavalan P et al.** Long-term follow-up of a large active surveillance cohort of patients with prostate cancer. *J Clin Oncol* 2015; 33: 272–7

9 **Tosoian JJ, Mamawala M, Epstein JI et al.** Intermediate and longer-term outcomes from a prospective active-surveillance program for favorable-risk prostate cancer. *J Clin Oncol* 2015; 33: 3379–85

10 **Gross MD, Sedrakyan A, Bianco FJ et al.** SPARED collaboration: patient selection for partial gland ablation in men with localized prostate cancer. *J Urol* 2019; 202: 952–8

11 **Le Nobin J, Rosenkrantz AB, Villers A et al.** Image guided focal therapy for magnetic resonance imaging visible prostate cancer: defining a 3-dimensional treatment margin based on magnetic resonance imaging histology co-registration analysis. *J Urol* 2015; 194: 364–70

12 **Weinreb JC, Barentsz JO, Choyke PL et al.** PI-RADS prostate imaging - reporting and data system: 2015, version 2. *Eur Urol* 2016; 69: 16–40

13 **Tay KJ, Scheltema MJ, Ahmed HU et al.** Patient selection for prostate focal therapy in the era of active surveillance: an International Delphi Consensus Project. *Prostate Cancer Prostatic Dis* 2017; 20: 294–9

14 **Hansen NL, Barrett T, Koo B et al.** The influence of prostate-specific antigen density on positive and negative predictive values of multiparametric magnetic resonance imaging to detect Gleason score 7–10 prostate cancer in a repeat biopsy setting. *BJU Int* 2017; 119: 724–30

15 **Zhang Z, Wu HH, Priester A et al.** Prostate microstructure in prostate cancer using 3-T MRI with diffusion-relaxation correlation spectrum imaging: validation with whole-mount digital histopathology. *Radiology* 2020; 296: 348–55

16 **Wildeboer RR**, **van Sloun RJG**, **Wijkstra H**, **Mischi M**. Artificial intelligence in multiparametric prostate cancer imaging with focus on deep-learning methods. *Comput Methods Programs Biomed* 2020; 189: 105316
17 **Schned AR**, **Wheeler KJ**, **Hodorowski CA et al.** Tissue-shrinkage correction factor in the calculation of prostate cancer volume. *Am J Surg Pathol* 1996; 20: 1501–6
18 **Schmid HP**, **McNeal JE**. An abbreviated standard procedure for accurate tumor volume estimation in prostate cancer. *Am J Surg Pathol* 1992; 16: 184–91
19 **Aslim EJ**, **Law YM**, **Tan PH et al.** Multiparametric MRI reporting using Prostate Imaging Reporting and Data System version 2.0 (PI-RADSv2) retains clinical efficacy in a predominantly post-biopsy patient population. *Asian J Urol* 2019; 6: 256–63
20 **Tan N**, **Lin WC**, **Khoshnoodi P et al.** In-Bore 3-T MR-guided transrectal targeted prostate biopsy: prostate imaging reporting and data system version 2-based diagnostic performance for detection of prostate cancer. *Radiology* 2017; 283: 130–9
21 **Le JD**, **Tan N**, **Shkolyar E et al.** Multifocality and prostate cancer detection by multiparametric magnetic resonance imaging: correlation with whole-mount histopathology. *Eur Urol* 2015; 67: 569–76
22 **Stamey TA**, **Freiha FS**, **McNeal JE**, **Redwine EA**, **Whittemore AS**, **Schmid HP**. Localized prostate cancer. Relationship of tumor volume to clinical significance for treatment of prostate cancer. *Cancer* 1993; 71: 933–8
23 **Tay KJ**, **Gupta RT**, **Brown AF**, **Silverman RK**, **Polascik TJ**. Defining the incremental utility of prostate multiparametric magnetic resonance imaging at standard and specialized read in predicting extracapsular extension of prostate cancer. *Eur Urol* 2016; 70: 211–3
24 **Gaziev G**, **Wadhwa K**, **Barrett T et al.** Defining the learning curve for multiparametric magnetic resonance imaging (MRI) of the prostate using MRI-transrectal ultrasonography (TRUS) fusion-guided transperineal prostate biopsies as a validation tool. *BJU Int* 2016; 117: 80–6
25 **Tay KJ**. Prostate focal therapy: the rule or exception? *Curr Opin Urol* 2018; 28: 512–21
26 **Bomers JGR**, **Cornel EB**, **Futterer JJ et al.** MRI-guided focal laser ablation for prostate cancer followed by radical prostatectomy: correlation of treatment effects with imaging. *World J Urol* 2017; 35: 703–11
27 **Lebastchi AH**, **George AK**, **Polascik TJ et al.** Standardized nomenclature and surveillance methodologies after focal therapy and partial gland ablation for localized prostate cancer: an international multidisciplinary consensus. *Eur Urol* 2020; 78: 371–8
28 **Tay KJ**, **Amin MB**, **Ghai S et al.** Surveillance after prostate focal therapy. *World J Urol* 2019; 37: 397–407
29 **Karavitakis M**, **Ahmed HU**, **Abel PD**, **Hazell S**, **Winkler MH**. Tumor focality in prostate cancer: implications for focal therapy. *Nat Rev Clin Oncol* 2011; 8: 48–55
30 **Ahmed HU**, **Dickinson L**, **Charman S et al.** Focal ablation targeted to the index lesion in multifocal localised prostate cancer: a prospective development study. *Eur Urol* 2015; 68: 927–36
31 **Gupta RT**, **Brown AF**, **Silverman RK et al.** Can radiologic staging with multiparametric MRI enhance the accuracy of the partin tables in predicting organ-confined prostate cancer? *AJR Am J Roentgenol* 2016; 207: 87–95

Correspondence: Kae Jack Tay, Department of Urology, Singapore General Hospital, Level 5, The Academia, 20 College Road, Singapore 169856, Singapore.

e-mail: tay.kae.jack@singhealth.com.sg

Abbreviations: FT, focal therapy; GS, Gleason score; HG, high grade; ICC, intraclass correlation coefficient; LG, low grade; mpMRI, multiparametric MRI.

Supporting Information

Additional Supporting Information may be found in the online version of this article:

Table S1. Multiparametric MRI acquisition protocols.
Table S2. Tumour distribution by location.
Fig. S1. Plot of size discrepancies (MRI minus histology) against entire tumour size on histology.